INFORMATICS JOURNALS

ISSN (Print) : 0013-466X
ISSN (Online) : xxxx-xxxx

The Journal of Electrochemical Society of India, Volume 75, Issue (2), April-June 2026; pp. 82-105

DOI: 10.18311/JESCI/2026/56362

Influence of Water Contamination on the Corrosion of Nickel Alloy in Biodiesel

Siddharth Atal[1], Ajeet Kumar Prajapati[1], Pranav Kumar[1], Saurabh Kumar[1], Kuncha Swaraj[1], Rakesh Kumar[1], Harish Hirani[2] and Deepak Dwivedi[1]*

[1]Department of Chemical and Biochemical Engineering, Rajiv Gandhi Institute of Petroleum Technology, Jais Campus, Amethi - 229304, Uttar Pradesh, India

[2]Department of Mechanical Engineering, Rajiv Gandhi Institute of Petroleum Technology, Jais Campus, Amethi - 229304, Uttar Pradesh, India

Abstract

With the global transition towards cleaner energy, biodiesel is increasingly blended with conventional fuels such as gasoline and diesel. However, the inherent oxygen content of Fatty Acid Methyl Esters (FAMEs) and the high hygroscopicity of biodiesel increase the ionic conductivity of the fuel medium, creating an electrolytic environment that accelerates electrochemical dissolution, pitting, and oxide-scale formation on conventional carbon steel pipelines. In contrast, Ni alloy UNS718 (comprising ~52% Ni, ~18% Cr, ~3% Mo, and ~5% Nb) forms a stable, self-healing chromium-rich passive film supplemented by nickel ferrite (NiFe2O4) spinel layers, offering corrosion rates several orders of magnitude lower than those reported for carbon steel in similar biodiesel environments. This study systematically investigates the corrosion behaviour of UNS718 in Used Cooking Oil Biodiesel (UCOB) with controlled water contamination (0.1% and 1%) over immersion periods of 24, 48, and 120 h. Gravimetric analysis coupled with FESEM-EDS, XRD, XPS, and FTIR characterisation revealed that higher water content (1%) yielded the highest corrosion rate (CR) of 4.158 × 10- 6 mm/year after 120 h, whereas lower water content (0.1%) promoted the formation of a protective $NiFe_2O_4/Cr_2O_3$ surface oxide that reduced the CR to 2.80 × 10-6 mm/year between 48 and 120 h. XPS analysis confirmed the progressive development of thin/amorphous nickel ferrite passivation films, while the absence of corresponding crystalline peaks in XRD indicated film thicknesses below the diffraction detection limit. Electrochemical noise measurements further corroborated the formation of a stable barrier layer at lower water concentrations. These findings demonstrate that UNS718 exhibits exceptional resistance to general, pitting, and crevice corrosion in water-contaminated biodiesel, making it a promising candidate material for sustainable pipeline and storage-tank infrastructure in biofuel transport systems.

Keywords: Biodiesel, Corrosion Rate, Nickel Alloy UNS718, Passive Film, Pipeline Integrity, Used Cooking Oil, Water Contamination

1. Introduction

The upstream and downstream oil and gas industries handle aggressive chemicals where they require materials of construction which can process, store and transport such aggressive materials without any failure. Nickel-based alloys have proved their candidacy to be counted in the category of sustainable materials for handling such aggressive chemicals[1]. These alloys are crucial in situations that require reliability and performance, as these alloys have outstanding resistance to oxidation and corrosion in thermally and chemically severe environments[2,3]. Pipelines that transport highly corrosive fluids are normally exposed to hydrogen sulfide (H_2S), carbon dioxide (CO_2) and chloride ions, making the corrosive media redox in

*Author for correspondence

*Email: ddwivedi@rgipt.ac.in

nature. Therefore, the use of Corrosion Resistant Alloys (CRAs), especially Ni-based alloys, has become a possible option that provides corrosion resistance in both oxidising and reducing environments[1]. Inconel alloy 718 (UNS N07718) is one of the most commonly used Ni-based alloys in the oil and gas industries due to its excellent mechanical properties such as toughness, high strength, and oxidation resistance at elevated temperatures[4]. Its exceptional qualities have made it suitable for a variety of uses, including pipeline systems and oil well components[5]. Alloy 718 (UNS N07718) is one of the important grades of Ni-based alloys that have made their credentials in the oil and gas sector because of excellent toughness and good tensile strength, making it suitable for sophisticated applications involving wide temperature ranges from cryogenic to high-temperature conditions[6]. The upstream and downstream oil and gas industries handle aggressive chemicals, wherein they require materials of construction that can process, store, and transport such aggressive materials without any failure. Nickel-based alloys have proven their candidacy to be counted in the category of such sustainable materials for handling such aggressive chemicals.

Biofuels have been recommended as an alternative to the conventional crude-based fuels to reduce greenhouse gas emissions[7]. The oil and gas sector has undergone changes that have resulted in increased benefits and reduced logistics expenses through market-based changes. Pipeline owners can use the remaining capacity to transport other permitted liquids such as biofuels[8]. Currently, fuels are transported by trucks, trains and pipelines. Pipelines are considered one of the most reliable and cost-effective means of transporting biofuels considering cost-effectiveness, operational reliability and environmental sustainability. However, the use of existing crude-oil pipelines for transportation of biofuels is still problematic due to limitations imposed by the metallurgy and corrosion susceptibility of conventional pipeline materials[9,10].

Corrosion occurring in biodiesel storage and transportation systems is a major problem that impacts material integrity, fuel quality and operational safety. Biodiesel (primarily Fatty Acid Methyl Esters (FAMES)) has two inherent properties that contribute to corrosion: dissolved oxygen in ester functional groups, high hygroscopicity allowing water absorption, residual Free Fatty Acids (FFA) from incomplete transesterification, and trace metal contamination from processing[9,11]. The given factors combined create an environment with electrolytic properties that favor the electrochemical dissolution of conventional carbon steel infrastructure. In addition, water ingress through pipeline cracks, weldment defects, and storage tank seals leads to hydrolysis of FAMEs, resulting in more FFAs which further reduce the local pH and aggravate the corrosion[12,13]. Expected corrosion problems in biodiesel infrastructure are general (uniform) corrosion, localised pitting and crevice corrosion at flanges and at gasket joints, Microbiologically Influenced Corrosion (MIC) due to water accumulation at tank bottoms, and stress corrosion cracking under sustained tensile loading in corrosive environments[14,15].

There are multiple strategies that can be utilised to mitigate corrosion in biodiesel systems. To stabilise the fuel and reduce oxidative degradation of biodiesel and thus the formation of corrosive by-products, antioxidants (*e.g.*, butylated hydroxytoluene, tocopherols) and metal deactivators are added[16,17]. Material and coating selection comprises stainless steels, nickel-based alloys, and protective organic or inorganic coatings to isolate the metal substrate from the corrosive medium[9,18]. Corrosion inhibitors have been studied for biodiesel environments to inhibit anodic and cathodic reactions at the metal-fuel interface, such as imidazoline-based and phosphonate-based compounds[19]. Biocides, regular water drainage and tank cleaning protocols can control MIC caused by sulphate-reducing bacteria and fungi that thrive in water-contaminated biodiesel[16]. Furthermore, cathodic and anodic electrochemical protection methods, like sacrificial anodes and impressed

current systems, have been applied to protect large-scale storage infrastructure (Mitigating Corrosion Risks in Oil and Gas Equipment by Electrochemical Protection: Top of the Line Corrosion). However, the long-term performance of conventional carbon steel in biodiesel service is still unsatisfactory, and thus the search for corrosion resistant alloy systems is necessary.

Nickel-based alloys, particularly UNS N07718, provide an attractive solution to the corrosion problems experienced in biodiesel infrastructure. UNS718 has a unique multi-element composition (~52% Ni, ~18% Cr, ~3% Mo, ~5% Nb, and small additions of Ti and Al) which gives it superior corrosion resistance compared to ordinary carbon steel. Chromium forms a stable and self-healing Cr_2O_3 passive film that acts as the primary protection against general corrosion. The high nickel content stabilises the austenitic matrix, offering resistance to oxidative degradation in ester-rich environments[1,4]. Importantly, the presence of ~3 wt% molybdenum in UNS718 significantly improves the resistance to pitting and crevice corrosion in the presence of chloride and halide ions via enrichment of Mo^{6+} (as MoO_4^{2-}) species at film defect sites, blocking adsorption of aggressive anions and promoting rapid repassivation of metastable pits prior to transition to stable propagation[20,21]. The Pitting Resistance Equivalent Number (PREN = %Cr + 3.3×%Mo + 16×%N) of UNS718 is approximately 28, much higher than for carbon steel (PREN ≈ 0) and similar to super-austenitic stainless steels, confirming its superior resistance to localised corrosion[22]. Furthermore, the ~5 wt% niobium helps to stabilise the microstructure against sensitisation at grain boundaries during welding, thus reducing susceptibility to crevice corrosion at flange connections, gasket interfaces, and weld joints - areas particularly susceptible in pipeline infrastructure[6]. The synergistic effect of Cr (passive film formation), Mo (pitting corrosion inhibition and repassivation), Ni (matrix stability) and Nb (microstructural stabilisation) in oxidising environments with halide ions gives UNS718 excellent resistance to general and localized corrosion and makes it a better choice than carbon steel for biodiesel pipeline applications[1].

Novelty of the present work: There is extensive literature on the corrosion of traditional metals in biodiesel, but no systematic study has been performed on the effects of water-contaminated biodiesel on Ni alloy UNS718. The present work fills this gap by providing, for the first time, a comprehensive evaluation of the corrosion performance of UNS718 in UCOB with controlled water contamination (0.1% and 1%) for different immersion periods. The novelty of this work includes: (i) identification of critical water content threshold (0.1%) below which water promotes protective $NiFe_2O_4/Cr_2O_3$ passive film formation instead of accelerating corrosion; (ii) detection of thin/amorphous nickel ferrite spinel passivation layers by XPS that are below the XRD detection limit, mechanistically clarifying the passivation process; (iii) demonstration that 1% water content disrupts the protective film and accelerates corrosion establishing an upper safe-limit for water contamination in Ni alloy biodiesel pipelines; and (iv) integration of gravimetric, surface-analytical (FESEM-EDS, XRD, XPS, FTIR) and electrochemical noise (ECN/RCE) techniques to provide a multi-scale understanding of the corrosion mechanism. These findings provide mechanistic insights relevant to the design, material selection and integrity management of biodiesel transportation and storage infrastructure, thus supporting the worldwide transition toward renewable energy adoption.

2. Materials and Methods

2.1 Biodiesel Synthesis and Selection

The procedures for using High-Pressure-High-Temperature (HPHT) autoclave technology to produce UCOB are described in detail elsewhere[23]. In brief, the HPHT autoclave process involves subjecting the feedstock oils to elevated pressures and temperatures in a controlled environment, which enhances the transesterification reaction and improves the overall conversion efficiency. The selection of 100% UCOB

as the test medium is justified on three grounds. First, UCOB aligns with India's National Policy on Biofuels (2018), which prioritises non-edible and waste- derived feedstocks, and the Repurpose Used Cooking Oil (RUCO) initiative of FSSAI, which targets conversion of the estimated 5 billion litres of UCO generated annually into biodiesel[23]. Second, UCOB contains elevated levels of free fatty acids (5-15 wt%), residual moisture, and polar oxidation products relative to virgin-oil biodiesel, thereby representing a worst-case corrosive environment that yields conservative (safe-side) corrosion data for pipeline design[24-26]. Third, in operational practice, biodiesel is transported as B100 through dedicated pipelines prior to terminal blending; hence, evaluating neat biodiesel directly reflects service conditions encountered during pipeline transportation[27,28]. The present study extends our earlier work on Ni alloys in biodiesel without water (Prajapati, Saini, *et al.*, 2024) by specifically isolating the effect of controlled water contamination (0.1% and 1%) under identical experimental conditions.

2.2 Coupon Preparation

The corrosion resistance of the nickel alloy was assessed using used cooking oil (UCOB) (100%) 150 UNS718. To prepare for the examination, samples were extracted from nickel alloy rods acquired from M P Steel Solutions in Mumbai (material composition in Table 1). Test coupons measuring 11.9 mm in length, 11.9 mm in width, and 1 mm in thickness were machined and ground using round bars. Subsequently, they were refined utilising silicon carbide sheets (grades 400 to 1,200), cleaned with distilled water, decontaminated of grease using acetone, and desiccated with argon gas as outlined in research[29]. After that, each coupon was submerged for varying amounts of time in a fuel that contained 30 ml of biodiesel samples UCO 100% (*e.g.*, 24, 48 and 120 h) at 27±2°C, as shown in Figure 1. In order to remove any corrosion products, the coupons were cleaned using chemical pickling solutions, as recommended by ASTM G1-03 (2017) and ISO 8407:2021[30], following each immersion test. A digital balance (Model: MS402S) with a four-digit accuracy level was used to assess the weight loss of each coupon. To guarantee consistency and reduce error (experimental error in CR measurement of 1.5%), the corrosion test was carried out three times by weighing each sample three times. The procedures for using HPHT autoclave technology to produce UCOB are described in detail elsewhere[23]. In brief, the HPHT autoclave process involves subjecting the feedstock oils to elevated pressures and temperatures in a controlled environment, which enhances the transesterification reaction and improves the overall conversion efficiency. The selection of 100% UCOB as the test medium is justified on three grounds. First, UCOB aligns with India's National Policy on Biofuels (2018), which prioritises non-edible and waste- derived feedstocks, and the Repurpose Used Cooking Oil (RUCO) initiative of FSSAI, which

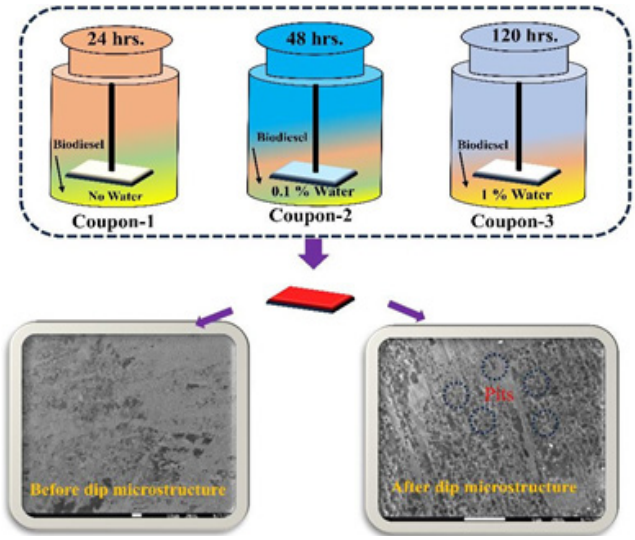


Figure 1. Coupon immersion setup.

targets conversion of the estimated 5 billion litres of UCO generated annually into biodiesel[23]. Second, UCOB contains elevated levels of free fatty acids (5-15 wt%), residual moisture, and polar oxidation products relative to virgin-oil biodiesel, thereby representing a worst-case corrosive environment that yields

conservative (safe-side) corrosion data for pipeline design[24-26]. Third, in operational practice, biodiesel is transported as B100 through dedicated pipelines prior to terminal blending; hence, evaluating neat biodiesel directly reflects service conditions encountered during pipeline transportation[27,28]. The present study extends our earlier work on Ni alloys in biodiesel without water (Prajapati, Saini, *et al.*, 2024) by specifically isolating the effect of controlled water contamination (0.1% and 1%) under identical experimental conditions.

2.3 Surface Examination and Spectroscopic Evaluation

After the immersion tests, the specimens were removed from the test solutions by the use of non-metallic tweezers, so as not to mechanically damage the corroded surfaces. Samples were immediately dried under a continuous flow of high-purity nitrogen gas to avoid air-drying artifacts and to suppress any post-immersion oxidation. The samples were then kept in a desiccator with fresh silica gel for at least 24 h to ensure complete removal of residual moisture prior to characterisation.

The surface morphology of pristine and corrosion Ni alloy specimens was studied by a Field-Emission Scanning Electron Microscope (FESEM, JSM-7900F, JEOL, Japan) equipped with an Energy Dispersive X-Ray Spectroscopy (EDS) detector. Qualitative elemental assessment, elemental cartography and Backscattered Electron (BSE) imaging were used to investigate the morphology, elemental distribution and compositional variations of the corrosion products formed on the alloy surface.

Further evaluation of the elemental composition of the immersed specimens was conducted using X-Ray Fluorescence (XRF) analysis (PANalytical LE neoR Fusion system (Claisse LE neo FLUXER)), which provides quantitative elemental information over a wide concentration range.

The phase composition of corrosion products was identified by X-Ray Diffraction (XRD) using an Empyrean-QTY1 diffractometer (Malvern PANalytical, Netherlands) with a Cu Kα radiation source (λ = 1.540 Å). Diffraction data were collected with a step of 0.007° in the range 2θ = 5°-90° to identify crystalline phases formed due to biodiesel exposure.

Chemical bonding characteristics and functional groups of corrosion products were analysed by Fourier-transform infrared spectroscopy (FTIR, Nicolet iS20, Thermo Fisher Scientific, USA). The spectra were collected in the spectral range 400–4000 cm^{-1}, with a spectral resolution of 0.25 cm^{-1}, and provided information on the organic and inorganic species formed on the alloy surface.

The surface chemical composition and oxidation states of the corrosion products were further investigated by X-ray photoelectron spectroscopy (XPS, K-Alpha, Thermo Fisher Scientific, USA) with a monochromatic Al Kα X-ray source at 14 kV and 15 mA. High-resolution spectra were recorded to identify the elemental composition and the chemical states of the species on surface responsible for the corrosion behaviour.

The combination of FESEM-EDS, XRF, XRD, FTIR and XPS offered a comprehensive insight into the morphological, elemental, structural and chemical evolution of the Ni alloy surface after immersion in

Table 1. Material compositions

Material description (%)	C	Si	Mn	P	S	Cr	Mo	Ni	Al	Co	Cu	Nb	Ti
Composition	0.043	0.220	0.240	0.009	0.010	18.200	2.960	52.260	0.410	0.550	0.210	4.982	0.790

biodiesel. These complementary characterisation techniques made it possible to correlate in detail the corrosion mechanisms with the composition, crystallinity and chemical nature of the corrosion products formed during exposure.

2.4 Corrosion Test

To assess whether the release of metal from the surface during the corrosion process has an impact on biodiesel stability, immersion tests were conducted using Ni Alloy UNS718 coupons with an area of 1.4176 cm^2. These tests were performed by immersing the coupons in UCO biodiesel with different proportions of water, as illustrated in Figure 1. The exposure time for the immersion tests was analysed in three stages: stage 1 (24 h), stage 2 (48 h), and stage 3 (120 h). The degree of corrosion was assessed by measuring the Corrosion Rate (CR) utilising the following Equation (1) in accordance with ASTM G1-03 (2017) and ISO 8407:2021 [31].

$$CR = \frac{K \times \Delta m}{\rho \times A \times T} \quad (1)$$

where K = 8.76 × 104 (for CR in mm/year, mass in g, area in cm^2, time in hours); Δm = weight loss (g); ρ = density (g/cm^3); A = exposed area (cm^2); T = exposure time (h) and the nickel alloy (UNS718) had a density of 8.19 g/cm^3, with an exposed surface area of 141.7 mm^2.

2.5 Electrochemical Testing of Corrosion using Rotating Cylinder Electrode (RCE)

The corrosion resistance of used cooking oil biodiesel samples was evaluated utilising a RCE method (ASTM G185). Each oil sample was subjected to rotation at 3000 RPM and sustained at ambient temperature for four hours. The electrochemical measurements were performed using a two-electrode setup including identical working electrodes and an Ag/AgCl reference electrode. The Electrochemical Noise (EN) measurements were conducted using a Metrohm Multilab Autolab M204 electrochemical workstation to quantify the noise (Atal *et al.*, 2026).

3. Results and Discussion

3.1 Analysis of Corrosion Rate

The weight loss method was used to calculate the CR. Following immersion, coupons began to lose weight, most likely as a result of oxidative interaction with the fuel samples, suggesting that ions were discharged from the metal surface into the fluid. The corrosion resistance of used cooking oil biodiesel samples was evaluated utilising an RCE method (ASTM G185). Each oil sample was subjected to rotation at 3000 RPM and sustained at ambient temperature for four hours. The electrochemical measurements were performed using a two-electrode setup including identical working electrodes and an Ag/AgCl reference electrode. The Electrochemical Noise (EN) measurements were conducted using a Metrohm Multilab Autolab M204 electrochemical workstation to quantify the noise (Atal *et al.*, 2026).

The corrosion resistance of Ni alloy (UNS718) subjected to all three mixtures of water and biodiesel, as

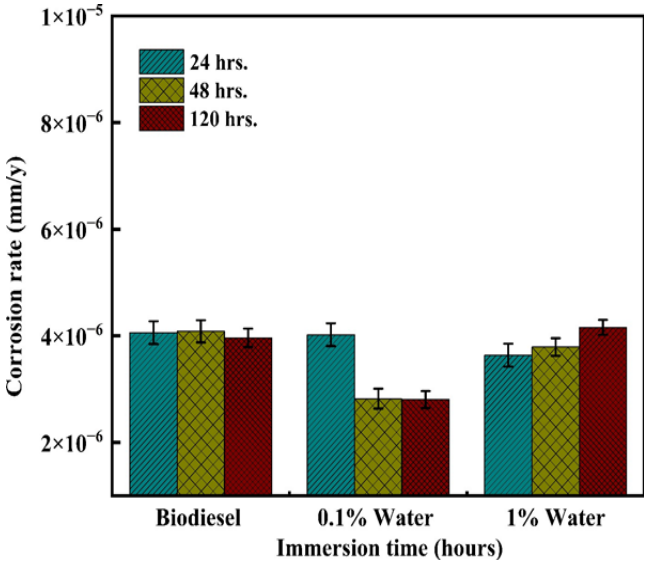


Figure 2. CR (measured in mm/year) of Ni alloy (UNS 718) exposed to UCOB for 24, 48, and 120 h.

well as solely biodiesel solutions, exhibited a consistent decrease with increasing immersion time, as depicted in Figure 2. Notably, the highest CR was observed in UCOB with 1% water addition after 120 h (4.15×10^{-6} mm/year), whereas the lowest rate occurred with 0.1% water addition (2.80×10^{-6} mm/year) in biodiesel at the same time point, highlighting significantly reduced corrosion compared to other biodiesel solutions and The present results are a continuation of our earlier published work[29] on biodiesel systems without water contamination. In contrast to that study, the current investigation focuses on water- contaminated biodiesel and reveals that a duration of five days is sufficient to evaluate both the CR and the associated corrosion patterns. Notably, the corrosion morphology and overall degradation trends observed after five days were found to be consistent with those recorded after longer exposure periods of one and two months. The plateau in CR observed after 48-120 h suggests the formation of a mass transfer-limiting barrier on the alloy surface. The surface characterisation techniques (XRD, XPS, and FESEM-EDS) described in Sections 3.2 to 3.4 and summed up in the corrosion mechanism (Section 4) underpin the specific composition, morphology, and protectiveness of this passive layer, and gravimetric analysis confirms the macroscopic reduction in metal dissolution.

3.2 X-ray Diffraction Analysis

XRD analysis was utilised to examine the corrosion products that developed on Nickel alloy (UNS 718) when subjected to UCOB. Figure 3(a-c) illustrates the visual appearance of various metal coupons exposed to the water-biodiesel mixture. Significantly, new peaks emerged in the samples with 0.1% water, 1% water, and UCOB (B100). A clear oxide layer developed on all samples following biodiesel exposure, except for B100 (24 h), where the peaks were more pronounced than those in the 0.1% and 1% water samples. The corrosion resistance of Ni alloy (UNS718) subjected to all three mixtures of water and biodiesel, as well as solely biodiesel solutions, exhibited a consistent

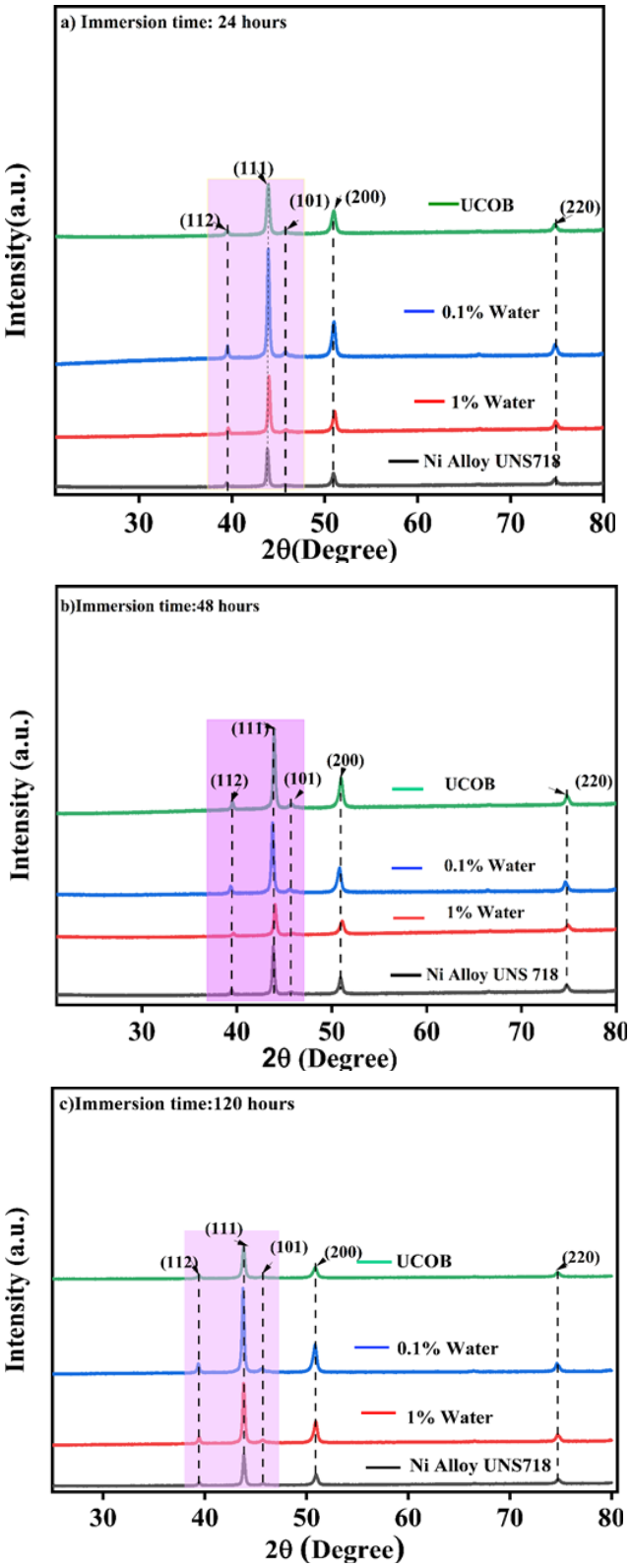


Figure 3. The XRD spectra of exposure times of **(a)** 24 h, **(b)** 48 h and **(c)** 120 h, respectively.

decrease with increasing immersion time, as depicted in Figure 2. Notably, the highest CR was observed in UCOB with 1% water addition after 120 h (4.15×10^{-6} mm/year), whereas the lowest rate occurred with 0.1% water addition (2.80×10^{-6} mm/year) in biodiesel at the same time point, highlighting significantly reduced corrosion compared to other biodiesel solutions and The present results are a continuation of our earlier published work[29] on biodiesel systems without water contamination. In contrast to that study, the current investigation focuses on water- contaminated biodiesel and reveals that a duration of five days is sufficient to evaluate both the CR and the associated corrosion patterns. Notably, the corrosion morphology and overall degradation trends observed after five days were found to be consistent with those recorded after longer exposure periods of one and two months. The plateau in CR observed after 48-120 h suggests the formation of a mass transfer-limiting barrier on the alloy surface. The surface characterisation techniques (XRD, XPS, and FESEM-EDS) described in Sections 3.2 to 3.4 and summarised in the corrosion mechanism (Section 4) underpin the specific composition, morphology, and protectiveness of this passive layer, and gravimetric analysis confirms the macroscopic reduction in metal dissolution.

To investigate the phase transformation that occurred while exposing the samples to different percentages of water addition in biodiesels for different time durations, XRD analysis of Ni alloys immersed in UCOB was performed as shown in Figure 3(a-c). Intriguingly, the nickel alloy submerged in UCOB till 120 h exhibited the emergence of TiN; however, there was no sign of strained corrosion product formation or change in the strain of the Ni alloy in comparison to the bare Ni alloy. This confirms either amorphous or very thin corrosion product formation (which was beyond the XRD's resolution limit). When Ni alloy samples were subjected to UCOB for 24 to 120 h, XPS examination revealed the presence of corrosion products as NiO, Fe_2O_3, MnO_2, Ni_2O_3, and $NiFe_2O_4$. It's noteworthy that the Ni alloy exposed to UCOB with 0.1% water addition exhibited the lowest rate of corrosion because passive or protective layers formed within 48 h and lasted for 120 h. Ni alloys subjected to 1% water addition in biodiesel for 120 h showed a sharp peak in all of the distinctive peaks and did not show any signs of corrosion product production. It is worth noting that the metals undergo oxidation due to the presence of oxygen and active oxygen atoms dissolved in biodiesel. This oxidation process led to the formation of metal oxides such as TiO_2, Cu_2O, Fe_2O_3, and others[32]. The protective layer of metal oxide acted as a barrier, preventing direct contact between the metal surface and oxygen atoms, as well as the oil sample[9]. However, water and fatty acids are also responsible for metallic corrosion and need to be considered[10]. Based on the XRD analysis, it is concluded that either very thin or amorphous corrosion products would have formed on the top of the Ni alloy. In addition to this, the Ni alloys exposed to biodiesel with 0.1 and 1% water for 24 and 48 h exhibited a shift in the characteristic peak, which suggests either the incoherency between the film and substrate or a metastable state of film formation.

3.3 X-ray Photoelectron Spectroscopy Analysis

3.3.1 Ni Alloy XPS Investigation after a 24-h Immersion in UCOB

XPS survey curve of samples immersed in UCOB for 24 h depicts the constituent elements with oxidation states as C1s, O1s, Si2p, Cr2p, Nb3d, Ni2p, and Mn2p. After doing graph zooming and peak fitting, peaks pertaining to a binding energy of 852.6 eV for Ni metal were obtained[33] as shown in Figure 4.

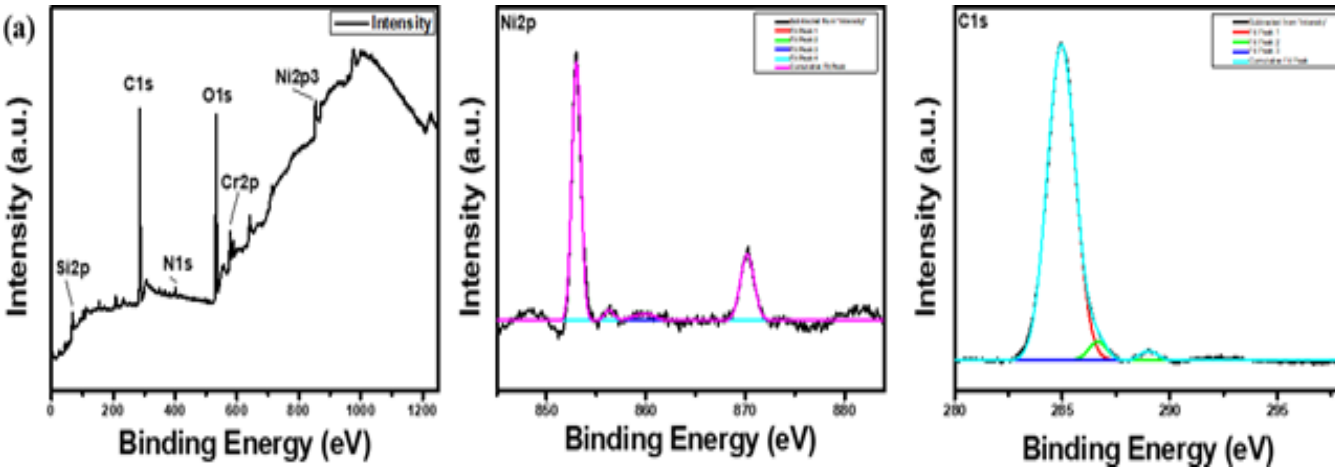


Figure 4. XPS spectra of the sample after 24 h of immersion in UCOB.

3.3.2 Ni alloy XPS investigation after a 48-h immersion in UCOB

XPS survey curve of samples immersed in UCOB for 24 h depicts the constituent elements with oxidation states as C1s, O1s, Si2p, Cr2p, Nb3d, Ni2p, and Mn2p. After graph zooming and peak fitting, peaks pertaining to the binding energies are obtained. The peaks at the binding energy of 852.6 in the Ni2p XPS spectra are attributed to Ni metal (Figure 5)[29,33].

3.3.3 Ni alloy XPS Investigation after a 120 h Immersion in UCOB

XPS survey curve for samples immersed in UCOB for 24 h depicts the constituent elements with oxidation states as C1s, O1s, Si2p, Cr2p, Nb3d, Ni2p3, and Mn2p. After doing graph zooming and peak fitting, Peaks pertaining to a binding energy of 852.6 eV for Ni metal and 856 eV for $NiFe_2O_4$[34,35] were observed, as shown in Figure 6.

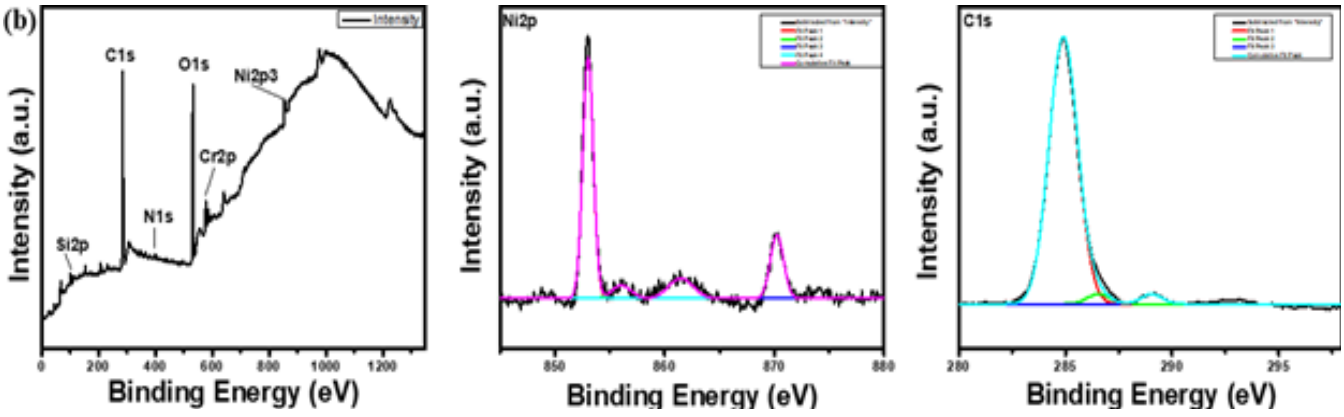


Figure 5. XPS spectra of the sample after 48 h of immersion in UCOB.

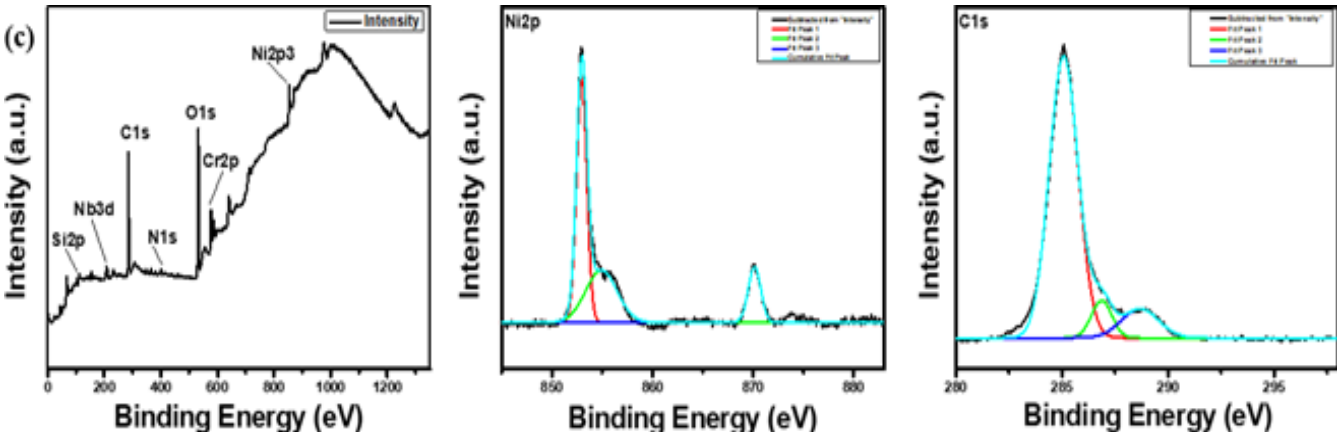


Figure 6. XPS spectra of the sample after 120 h of immersion in UCOB.

3.3.4 Ni Alloy Submerged in 0.1% Water for 24 h was Subjected to XPS Examination in UCOB

XPS survey curve for the pure sample of Ni Alloy (UNS718) depicts the constituent elements with oxidation states as C1s, O1s, Si2p, Nb3d, Cr2p, Ni2p and Mn2p. After doing graph zooming and peak fitting, Peaks corresponding to the binding energies were observed, with the metallic peaks at 852.6 eV for Ni being particularly evident, as shown in Figure 7. This observation is well in agreement with the research[36].

3.3.5 Ni Alloy Submerged in 0.1% Water for 48 h was Subjected to XPS Examination in UCOB

XPS survey curve for the pure sample of Ni Alloy (UNS718) depicts the constituent elements with oxidation states a C1s, O1s, Si2p, Nb3d, Cr2p, Ni2p, and Mn2p. After doing graph zooming and peak fitting, Peaks corresponding to the binding energies were observed, particularly the metallic peaks at 852.6 eV of Ni and 856 eV of $NiFe_2O_4$ [33-35] as shown in Figure 8.

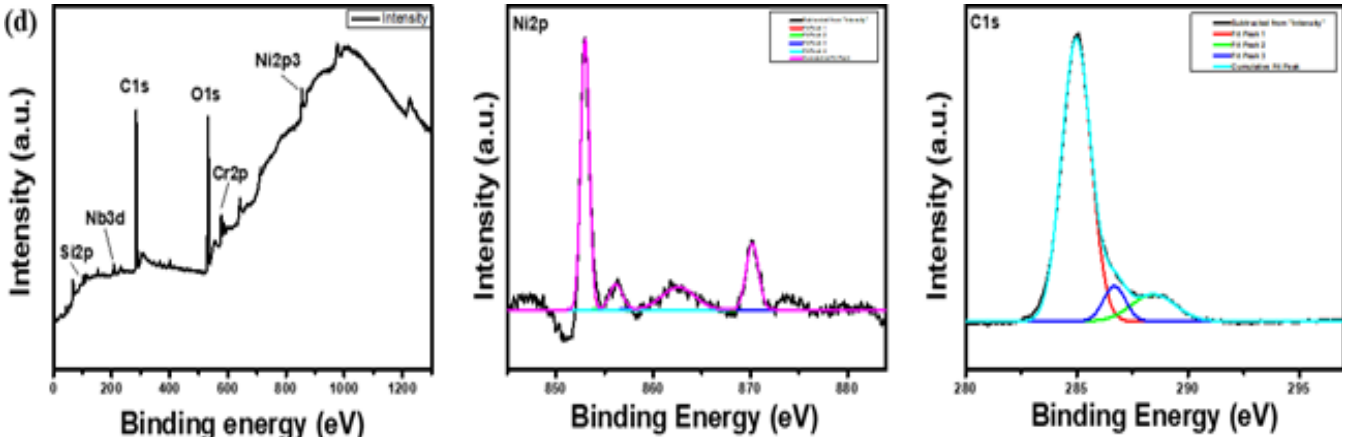


Figure 7. XPS spectra of the sample after 24 h of immersion in 0.1 % water addition on UCOB.

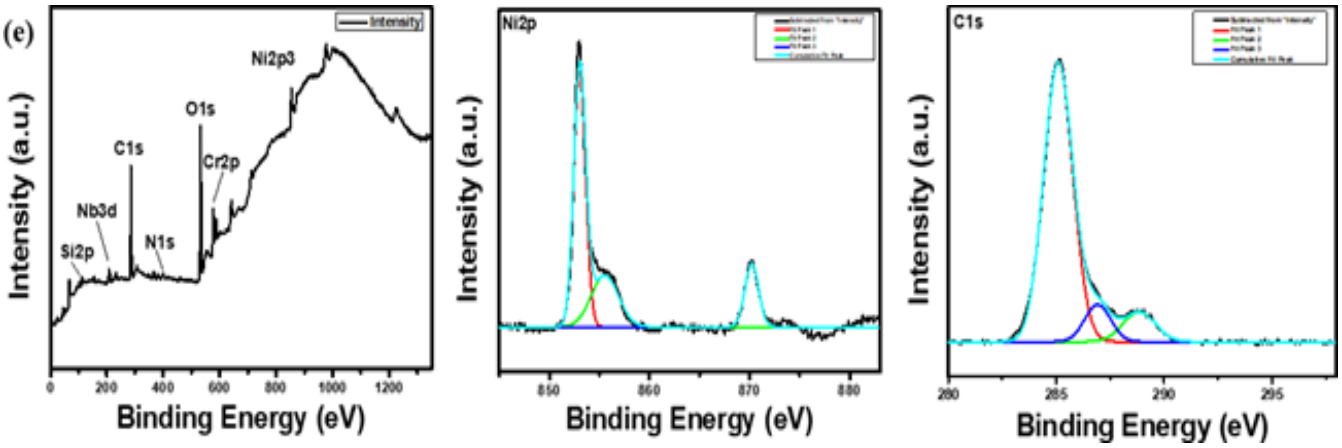


Figure 8. XPS spectra of the sample after 48 h of immersion in 0.1 % water addition on UCOB.

3.3.6 Ni Alloy Submerged in 0.1% Water for 120 h Was Subjected to XPS Examination in UCOB

XPS survey curve for the pure sample of Ni Alloy (UNS718) depicts the constituent elements with oxidation states as C1s, O1s, Si2p, Nb3d, Cr2p, Ni2p, and Mn2p. After doing graph zooming and peak fitting, Peaks corresponding to the binding energy were observed, particularly the metallic peaks at 852.6 eV for Ni metal and 856 eV for $NiFe_2O_4$, as shown in Figure 9.

3.3.7 XPS Investigation of Ni Alloy Submerged in 1% Water for 24 h in UCOB

XPS survey curve for the pure sample of Ni Alloy (UNS718) shows the elements with oxidation states as C1s, O1s, Si2p, Nb3d, Cr2p, Ni2p, and Mn2p. After doing graph zooming and peak fitting, Peaks corresponding to the binding energy were observed, with Ni2p exhibiting a metallic Ni peak at 852.6 eV and a $NiFe_2O_4$ peak at 856 eV, as shown in Figure 10.

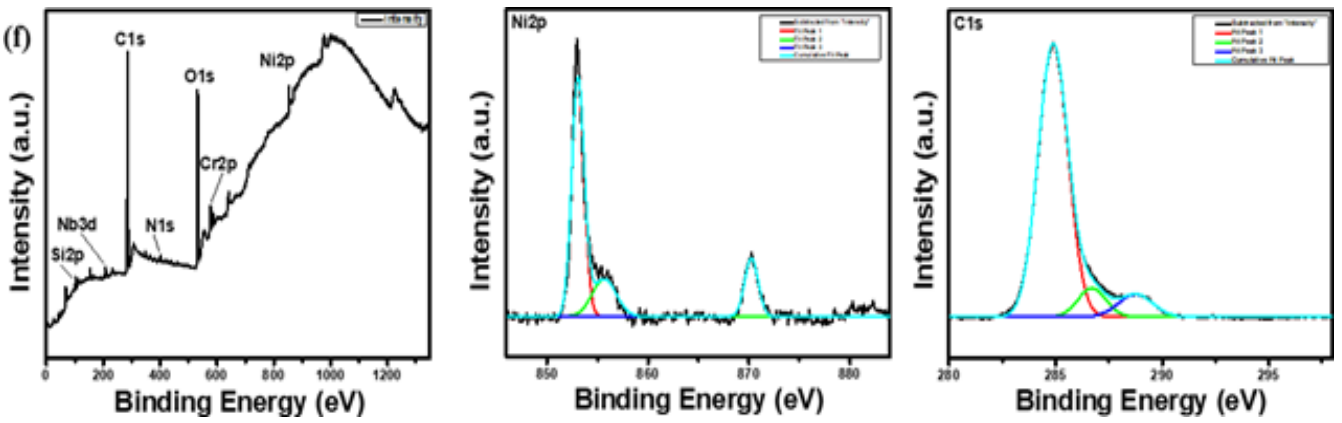


Figure 9. XPS spectra of the sample after 120 h of immersion in 0.1 % water addition on UCOB.

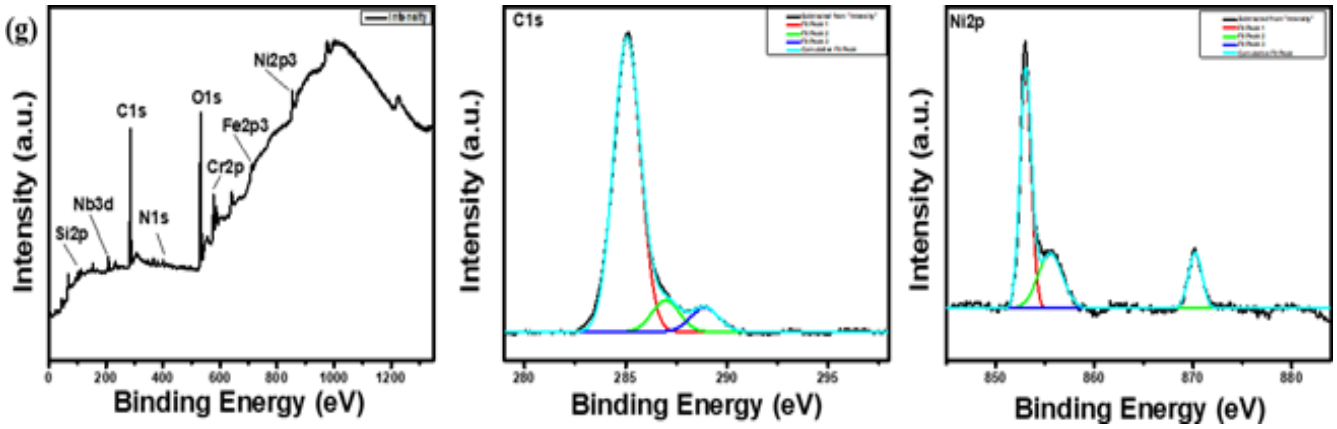


Figure 10. XPS spectra of the sample after 24 h of immersion in 1% water addition on UCOB.

3.3.8 XPS Investigation of Ni alloy Submerged in 1% Water for 48 h in UCOB

XPS survey curve for pure sample of Ni Alloy (UNS718) depicts the constituent elements with oxidation states as C1s, O1s, Si2p, Nb3d, Cr2p, Ni2p3 and Mn2p. After doing graph zooming and peak fitting, Peaks corresponding to the binding energy were observed, particularly the metallic peak at 852.6 eV and the $NiFe_2O_4$ peak at 856 eV from Ni2p, as shown in Figure 11.

3.3.9 XPS Investigation of Ni Alloy Submerged in 1% Water for 120 h in UCOB

XPS survey curve for the pure sample of Ni Alloy (UNS718) depicts the constituent elements with oxidation states as C1s, O1s, Si2p, Nb3d, Cr2p, Ni2p3 and Mn2p. After doing graph zooming and peak fitting, Peaks corresponding to the binding energies were observed, with the metallic peak at 852.6 eV of Ni for Ni2p, as shown in Figure 12.

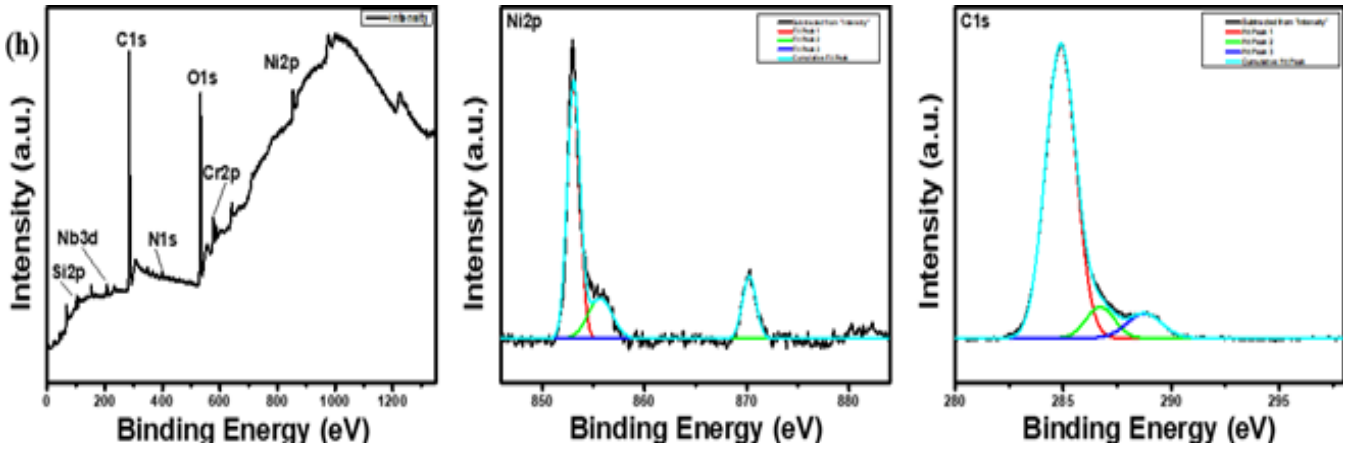


Figure 11. XPS spectra of the sample after 48 h of immersion in 1 % water addition on UCOB.

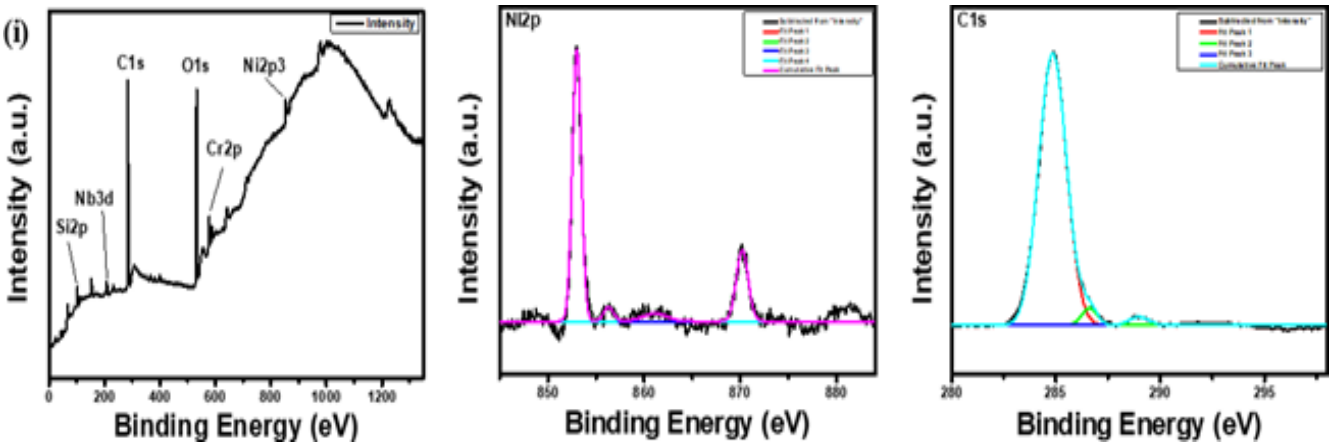
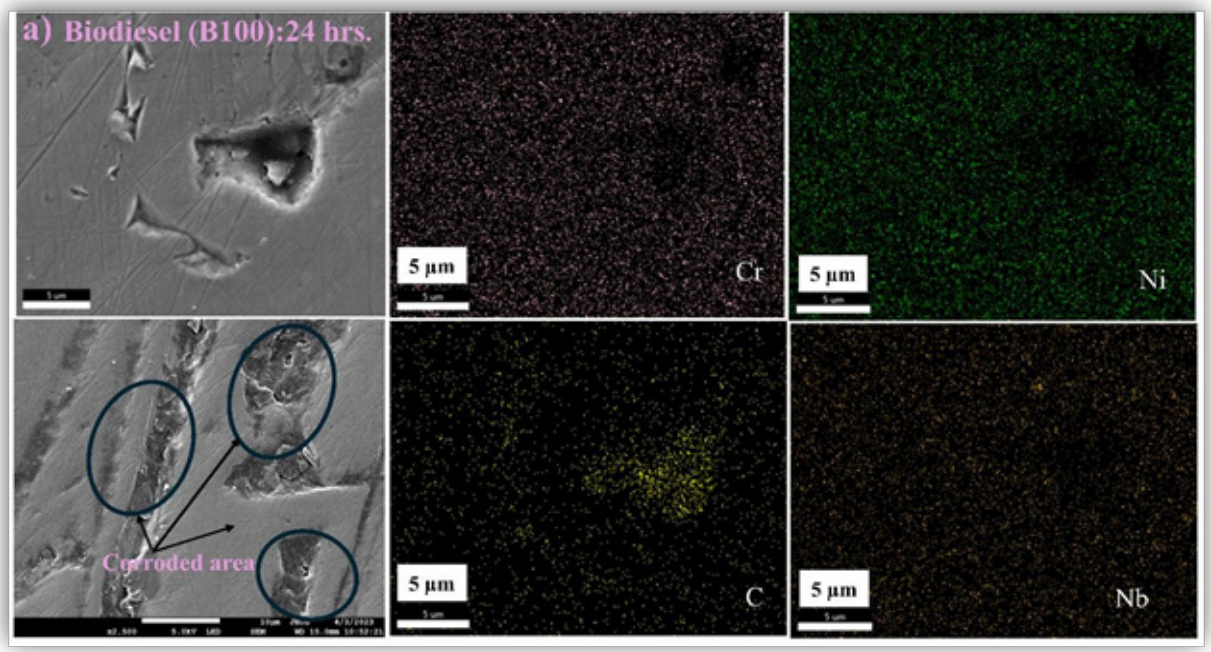


Figure 12. XPS spectra of the sample after 120 h of immersion in 1% water addition on UCOB.

3.4 Surface Morphology and Chemical Changes

3.4.1 Coupon Immersion in Biodiesel (B100)

The corrosion products' morphologies were examined using FESEM (Field Emission Scanning Electron Microscopy) and EDS (Energy-Dispersive X-ray Spectroscopy). As shown in Figure 13(a-c), the upper left panel illustrates the EDS elemental distribution, while the lower left panel presents the corresponding SEM micrograph highlighting the corroded regions of the specimen exposed to UCOB. The FESEM micrographs indicate that the metal surface undergoes a slight change due to corrosion after exposure to biodiesel. Several micro pits, appearing as dark spots, are observed on the metal surface and it is minimally influenced by the transesterification route. In Figure 13(a), the pits' varying sizes and distributions are evident, suggesting



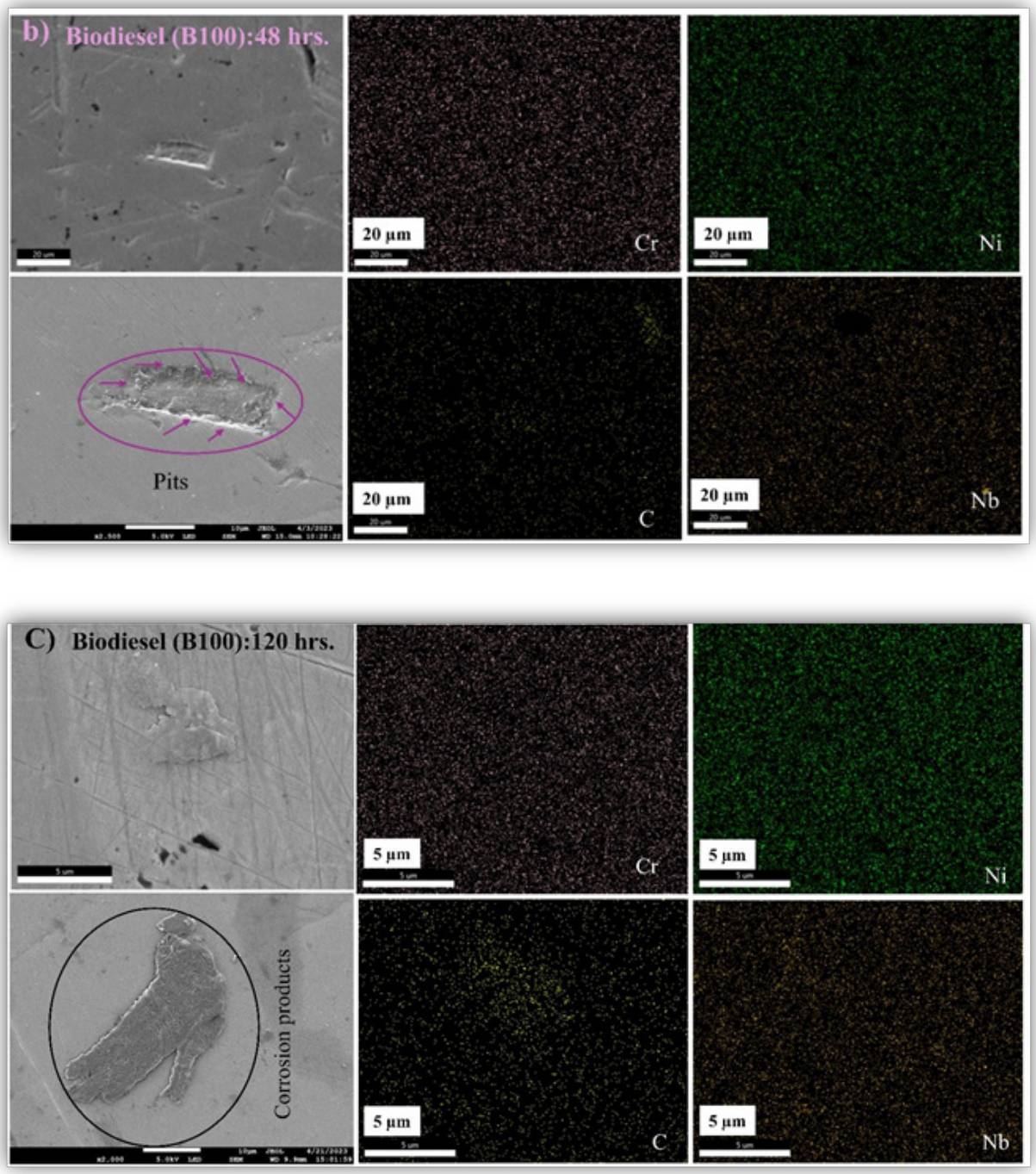


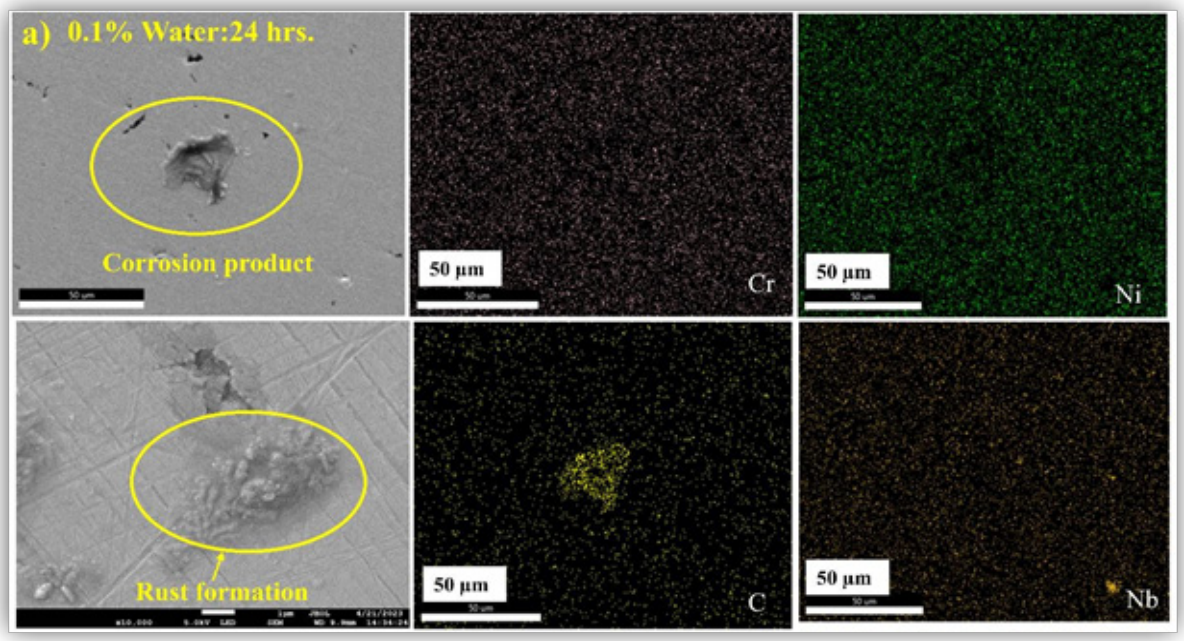
Figure 13. FESEM and EDS imaging of Ni alloy (UNS718) for biodiesel at exposure times **(a)** 24 h, **(b)** 48 h and **(c)** 120 h.

a dependence on the fuel's characteristics. The metal surface immersed in pure biodiesel (B100) without water exhibited a greater number of smaller pits for 24 h exposure time compared to the surfaces immersed in biodiesel at 48 and 120 h (Figure 13(b,c)). The results indicate that as the immersion time increases, the

formation of the oxide layer also increases (as exhibited by XPS and Figure 13(b,c)), leading to a decrease in the CR for B100 (48 h) and B100 (120 h). Ni alloy UNS718 is well- known for its corrosion resistance due to thin protective film formation on its surface. The reduced susceptibility of UNS718 to pitting corrosion is also influenced by the synergistic effect of major alloying elements (*e.g.*, ~18.2 wt% Cr and ~2.96 wt% Mo) in UNS718. Molybdenum is crucial in the destruction and reformation of the passive film. Chromium forms the primary protective oxide barrier. Upon localised film rupture, Mo enriches at the metal/solution interface and oxidises to insoluble molybdate species (*e.g.*, MoO_4^{2-}) that block the adsorption of aggressive anions and significantly enhance repassivation kinetics. The rapid repassivation hinders the transformation of the metastable micro-pits observed in FESEM into stable, propagating pits and therefore confers the alloy outstanding localised corrosion resistance in biodiesel environments. Following a 120-h immersion period, oxides of Fe and Cr were observed on the surfaces of the nickel alloy UNS718, as indicated by EDS mapping. It is interesting to note that these oxides were not observed through XPS, which could be attributed to either thick layer formation, due to which they were beyond the resolution limit of XPS, or missing the same as ROI.XPS survey curve for pure samples of Ni Alloy (UNS718) depicts the constituent elements with oxidation states as C1s, O1s, Si2p, Nb3d, Cr2p, Ni2p3 and Mn2p. After doing graph zooming and peak fitting, Peaks corresponding to the binding energies were observed, with the metallic peak at 852.6 eV of Ni for Ni2p, as shown in Figure 12.

3.4.2 Coupon Immersion in 0.1% Water Addition in Biodiesel

According to Brandao *et al.*[37], micro pitting is typically characterised by small pits with dimensions around 10 micrometres in width and depth. Vogiatzis *et al.*[38] proposed a model to explain the formation of micro pits. When immersed in fuel, the corrosion products create a relatively stable layer on the surface of the disc, leading to the formation of micro pits. This layer acts as a "protective film" that reduces the CR, as depicted in Figure 14; the upper left panel illustrates the EDS elemental distribution, while the lower left panel



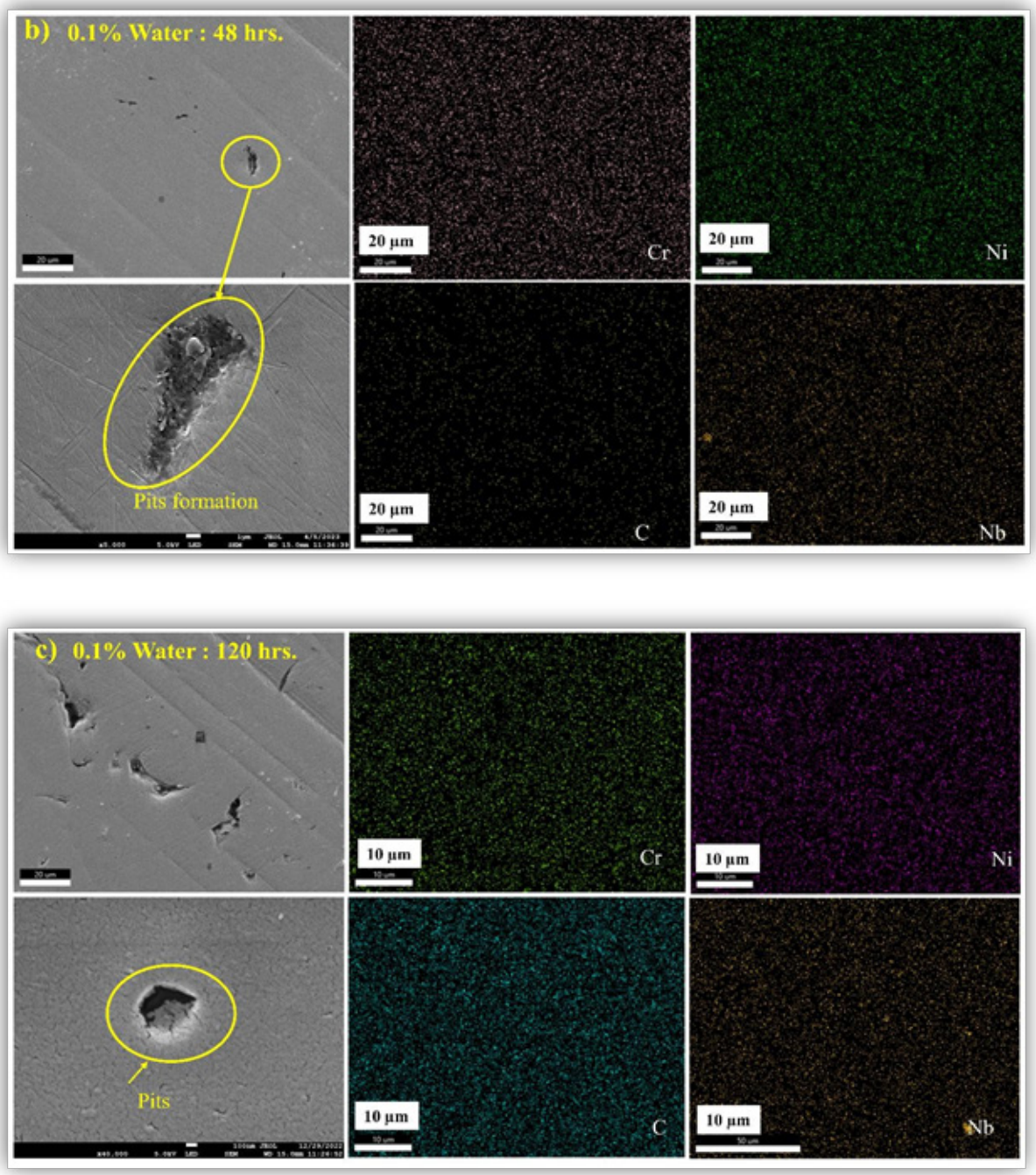


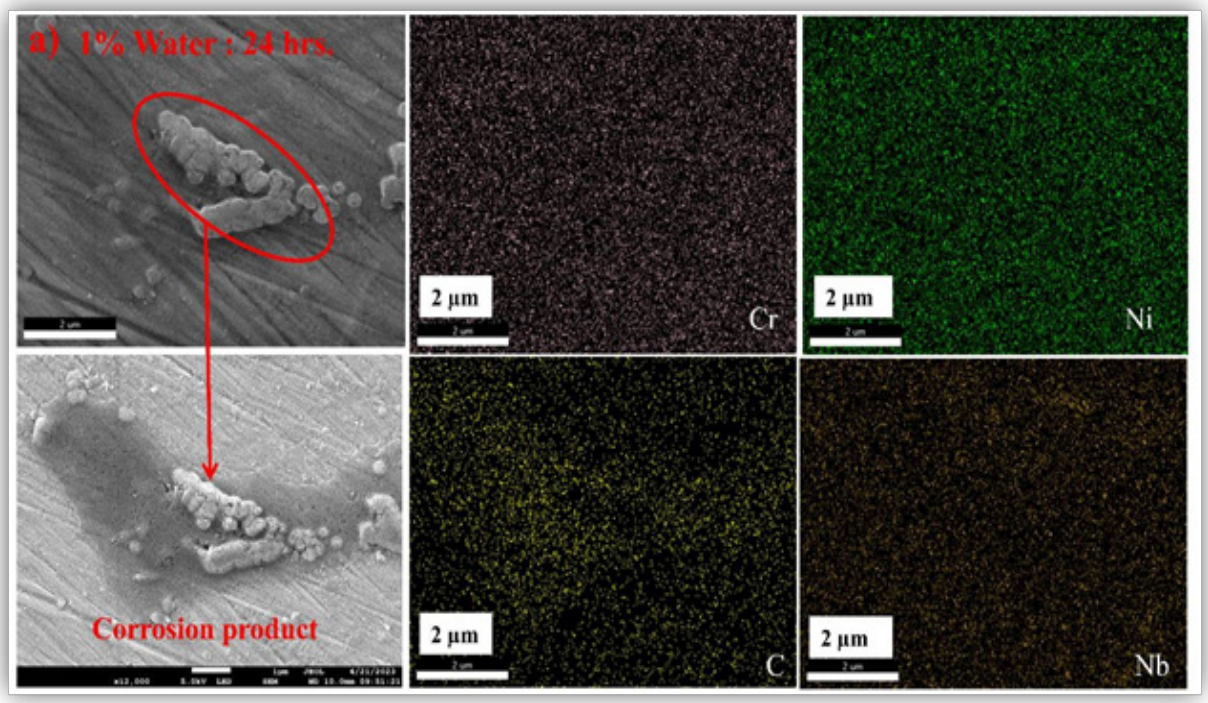
Figure 14. FESEM and EDS imaging of Ni alloy (UNS718) for 0.1% water addition exposure time: **(a)** 24 h, **(b)** 48 h and **(c)** 120 h.

presents the corresponding SEM. The presence of an oxide layer is primarily observed in samples exposed to 0.1% water for 24, 48, and 120 h, as confirmed by EDS analysis showing the distribution of oxygen across the entire surface, with a higher intensity in areas with micro-pitting. According to this correlation, the

CR reduces as exposure or immersion time increases (Figure 14(a-c)); the formation of the oxide layer becomes more pronounced. According to Brandao *et al.*[37], micro-pitting is typically characterised by small pits with dimensions around 10 micrometres in width and depth. Vogiatzis *et al.*[38] proposed a model to explain the formation of micro pits. When immersed in fuel, the corrosion products create a relatively stable layer on the surface of the disc, leading to the formation of micro pits. This layer acts as a "protective film" that reduces the CR, as depicted in Figure 14; the upper left panel illustrates the EDS elemental distribution, while the lower left panel presents the corresponding SEM. The presence of an oxide layer is primarily observed in samples exposed to 0.1% water for 24, 48, and 120 h, as confirmed by EDS analysis showing the distribution of oxygen across the entire surface, with a higher intensity in areas with micro-pitting. According to this correlation, the CR decreases as exposure or immersion time increases (Figure 14(a-c)); the formation of the oxide layer becomes more pronounced.

3.4.3 Coupon Immersion in 1% Water Addition in Biodiesel

The behaviour of the surface immersed in biodiesel differs due to the predominance of oxide layer formation in areas with micro-pitting, which can be observed as black dots on the metal surface. Furthermore, when the percentage of water, such as 1% water, was increased and tested at different immersion times (24, 48, and 120 h), it was observed that initially the CR was 3.63804×10^{-6} mm/year at 24 h; after that, it increased to 4.1582×10^{-6} mm/year at 120 h. This is because, as shown, there is no indication that a stable oxide layer is present on the coupons' upper surface in Figures 15(a-c), and the upper left panel illustrates the EDS elemental distribution, while the lower left panel presents the corresponding SEM. The behaviour of the surface immersed in biodiesel differs due to the predominance of oxide layer formation in areas with micro-pitting, which can be observed as black dots on the metal surface. Furthermore, when the percentage of water, such as 1% water, was increased and tested



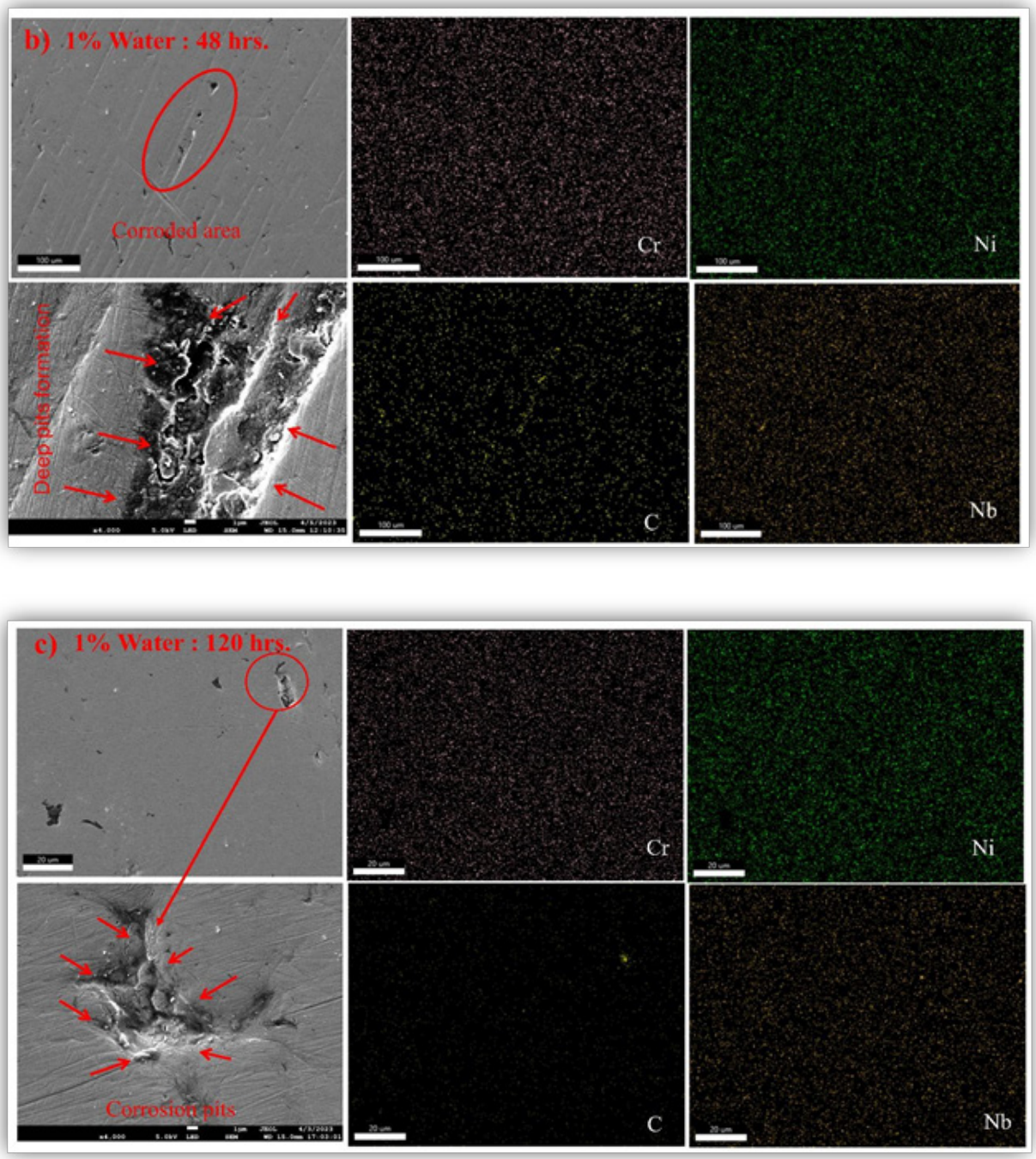


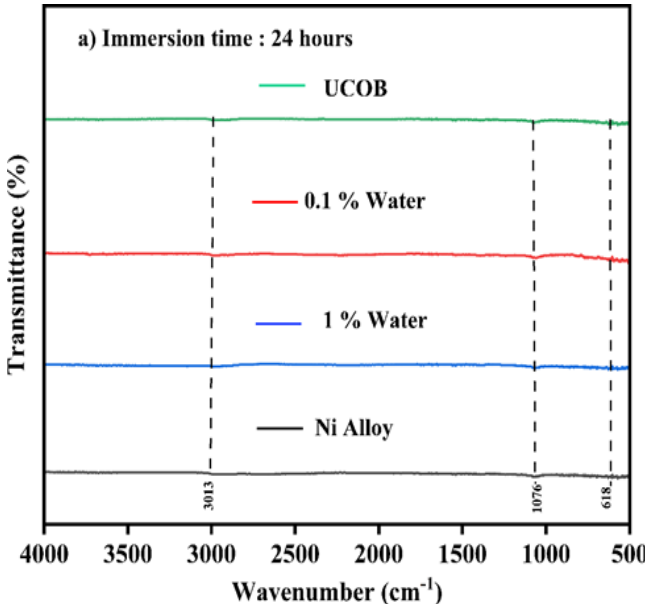
Figure 15. FESEM and EDS imaging of Ni alloy (UNS718) for 1% water addition exposure time: **(a)** 24 h, **(b)** 48 h and **(c)** 120 h.

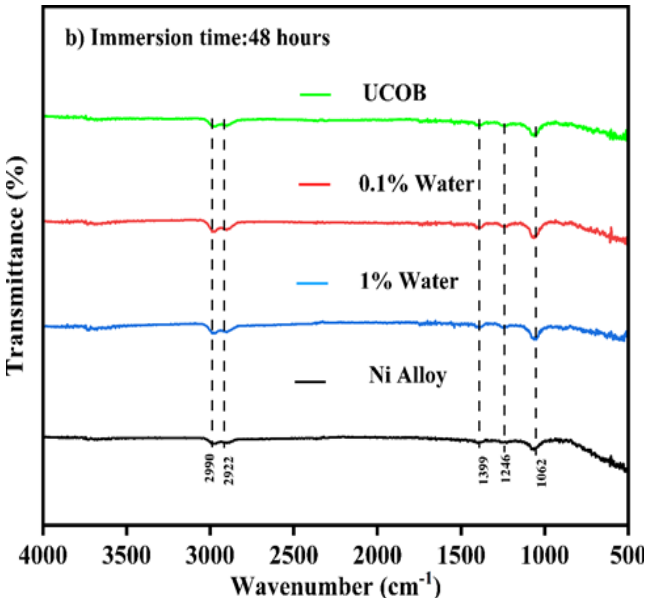
at different immersion times (24, 48, and 120 h), it was observed that initially the CR was 3.63804×10^{-6} mm/year at 24 h; after that, it increased to 4.1582×10^{-6} mm/year at 120 h. This is because, as shown, there is no indication that a stable oxide layer is present on the coupons' upper surface in Figures 15(a-c), and

the upper left panel illustrates the EDS elemental distribution, while the lower left panel presents the corresponding SEM.

3.5 Functionality of Surface using FTIR

The FTIR (Fourier Transform Infrared) spectroscopy method used in this study enabled the monitoring of chemical changes in biodiesel fuel samples over time by analysing specific peaks in the spectrum. Prior to exposure to test coupons, the infrared spectra of the fuel samples exhibited typical biodiesel regions, with variations in water content (0.1% and 1%), pure biodiesel (B100), and pure Ni Alloy UNS718 (without immersion samples), as shown in Figure 16(a-c). At an immersion time of 24 h (Figure 16a), no significant peaks were observed; however, minor peaks in the spectrum at 618 cm^{-1}, 1076 cm^{-1}, and 3013 cm^{-1} were assigned. These peaks correspond to the following vibrations: 618 cm^{-1} is attributed to C-H deformation, 1076 cm^{-1} to C-O stretching vibrations, and 3013 cm^{-1} to the stretching vibrations of carboxylic acids overlapping with C-H bonds. This clearly shows that during the 48-h immersion period, five significant peaks were observed in the spectrum, as depicted in Figure 16b. These peaks were recorded at 1062 cm^{-1}





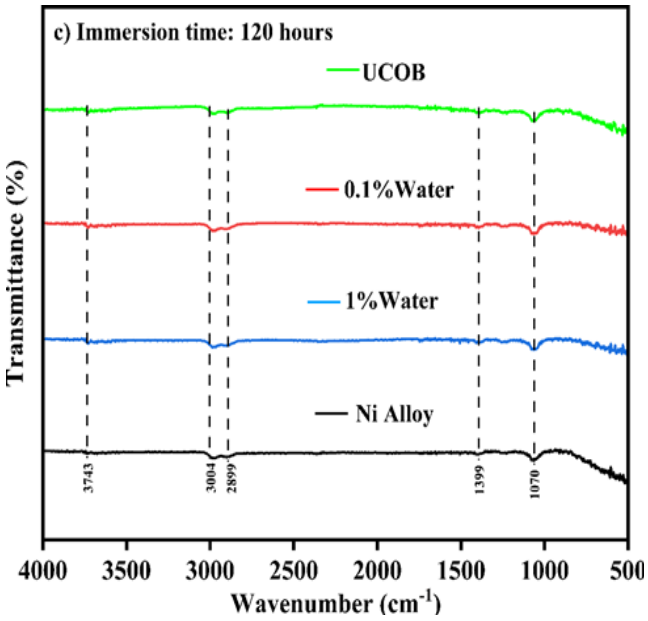


Figure 16. FTIR Spectra: **(a)** Immersion time 24 h, **(b)** Immersion time 48 h and **(c)** Immersion time 120 h.

(O-C stretching vibrations), 1246 cm^{-1} (O-C stretching vibrations), 1339 cm^{-1} (O-H in-plane bending), 2922 cm^{-1}, and 2990 cm^{-1} (stretching vibrations of CH_3, CH_2, and CH in alkanes) (Zhou *et al.*, 2017).

Figure 16(c) shows five significant peaks in the spectrum at 1070 cm^{-1}, 1399 cm^{-1}, 2899 cm^{-1}, 3004 cm^{-1}, and 3743 cm^{-1}. The presence of the C-O bond,

which belongs to the O-CH_3 group of long-chain methyl esters, has been confirmed by the appearance of a peak at 1070 cm^{-1} [17]. However, the presence of C-O-H bending was confirmed through a peak at 1399 cm^{-1}. The carboxylic groups were confirmed through the peaks at 2899 cm^{-1}, 3004 cm^{-1}, and 3743 cm^{-1}, which are attributed to broad O-H stretching vibrations.

3.6 Electrochemical Corrosion Evaluation Using ECN Using Rotating Cylinder Electrode (RCE) Technique

The corrosion resistance of biodiesel (UCO) samples with varying water percentages was evaluated using ECN (Electrochemical Noise study) using the RCE method[39]. Each oil sample was subjected to rotation at 3000 RPM and held at room temperature for four hours. While testing, assessment of principal corrosion indicators: Noise Resistance (NR), Open-Circuit Potential (OCP), and CR were obtained and listed in Table 2.

The data presented in Table 2 demonstrate distinct behavioural variations among the formulations. The pure Biodiesel (UCO) exhibited the highest CR of 3.69 $\times 10^{-6}$ mm/year, accompanied by a comparatively lower noise resistance of 1.63 ×10 8 Ω·cm^2 and an Open Circuit Potential (OCP) of -0.024 V.

A significant reduction in corrosion rate was observed with the increasing addition of water in pure biodiesel (UCO), with the maximum corrosion resistance recorded in the biodiesel sample containing 1% water, exhibiting the lowest CR of 4.9 × 10^{-7} mm/year, alongside a relatively high noise resistance of 1.23 × 109 Ω·cm^2 and an Open Circuit Potential (OCP) of -0.096 V. The results indicate that CR diminished with the increased addition of water to pure biodiesel (UCO).

The improved performance of the 1% water-added biodiesel (UCO) sample, exhibiting a higher noise resistance value, indicates the formation of a stable protective barrier on the metal surface, hence restricting corrosive reactions.

4. Corrosion Mechanism

The corrosion behaviour of the alloy in water blended UCOB is controlled by the water content, the exposure time and the progressive formation of a protective surface film. Within the first 24 h, the native oxide layer breaks down locally at surface defects, grain boundaries, and inclusions. The presence of water and polar components of biodiesel favours localised electrochemical processes. The higher ionic conductivity due to 1% water favours initial metal dissolution[12,15]. The selective dissolution of alloying elements takes place between 24 and 48 h with the formation of intermediate oxide species. Chromium promotes the formation of Cr rich oxide nuclei, whereas nickel and iron promote the formation of a mixed oxide phase[11]. Interestingly, the acceleration of the corrosion rate of UCOB with 0.1% water in this interval indicates that passivation at early stages is sensitive to the

Table 2. Electrochemical variables and CR of biodiesel (UCO) samples determined by RCE at room temperature and 3000 RPM

Sample	NR (Ω·cm^2)	CR (mm/year)	OCP (V)
Biodiesel (UCO)	1.63 E +08	3.69 E -06	-0.096
Biodiesel with 0.1% water addition	3.69 E +08	1.63 E -06	-0.031
Biodiesel with 1% water addition	1.23 E +09	4.9 E -07	-0.024

water- mediated surface interactions and competitive adsorption of water and organic species.

UCOB with 0.1 wt % water shows the lowest corrosion rate for 48–120 h, implying that a more effective passive film is formed. X-ray Photoelectron Spectroscopy (XPS) shows Ni^{2+} species and a high binding energy Ni component at ca. 856 eV, which is attributed to $NiFe_2O_4$ related species, suggesting the formation of a nickel iron oxide rich outer layer[11,16,19]. The corresponding FESEM–EDS mapping reveals an increase in oxygen coverage and enrichment of chromium and iron at the surface and the Cr2p signal observed in the XPS survey spectra further confirm the presence of chromium-containing surface species. Taken together, these results are consistent with a bilayered passive film comprising a Cr rich oxide layer as the primary barrier to mass transport and an outer layer of mixed nickel-iron oxide, possibly containing adsorbed organic species derived from biodiesel degradation. X-Ray Diffraction (XRD) did not show distinct crystalline peaks of corrosion products indicating that these products are present as a thin film which is poorly crystalline or amorphous in nature. However, the exact phase constitution cannot be determined by XRD alone.

The progressive stabilisation of the surface is indicated by higher surface oxygen coverage and lower micro-pit density with the growth of the passive film. The compact Cr rich inner layer prevents the outward migration of metal ions and restricts the transport of water and other aggressive species to the alloy surface. Consequently, the corrosion process tends toward a transport-limited regime where the dissolution of the metal is balanced by the growth and repassivation of the film, resulting in the observed stabilisation of the macroscopic corrosion rate. Thus, the improved performance of UCOB with 0.1% water signifies the optimal trade-off between the hydration needed for the oxide-film development and the increased corrosivity with high moisture content. Higher water content may also favour the formation of other aggressive degradation products and increase the ionic conductivity, which can prevent the persistence of the protective film.

5. Conclusion

This study systematically evaluated the corrosion properties of Ni alloy UNS718 in UCOB with controlled water contamination (0.1% and 1%) over immersion periods of 24, 48, and 120 h. The following key conclusions are drawn:

(i) UCOB with 1% water exhibited the highest corrosion rate (4.158×10^{-6} mm/year at 120 h), while 0.1% water promoted the formation of a protective passive film, reducing the CR to 2.80×10^{-6} mm/year.

(ii) XPS analysis confirmed the formation of a nickel ferrite ($NiFe_2O_4$) spinel passivation layer (~856 eV), while EDS mapping revealed chromium and iron oxide accumulation. The absence of crystalline corrosion peaks in XRD indicated that the passive film is ultra-thin or amorphous (<5 nm).

(iii) A critical water content threshold was identified: 0.1% water provides sufficient hydration for passive film maturation without triggering the aggressive electrolytic conditions and FAME hydrolysis associated with 1% water.

(iv) The superior corrosion resistance of UNS718 (CR ~10^{-6} mm/year) compared to conventional carbon steel (CR ~10^{-3}–10^{-2} mm/year) is attributed to the synergistic action of Cr (passive film), Mo (pitting inhibition), Ni (matrix stability), and Nb (microstructural stabilisation).

These findings provide mechanistic insights essential for the design, material selection, and integrity management of biodiesel transport and storage infrastructure, supporting the global transition towards renewable energy adoption.

6. Acknowledgement

We greatly acknowledge the Rajiv Gandhi Institute of Petroleum Technology provided for the experimental and technical support. The author would like to thank the CIF facility and its staff. Thanks are also extended to all the members associated with the work, and DD and RK acknowledge RGIPT for providing the necessary support for conducting experiments. DD acknowledges KAPL-Cristol for awarding the chair professorship and supporting the independent research activities under this chair.

7. References

1. Darolia R. Development of strong, oxidation and corrosion resistant nickel-based superalloys: Critical review of challenges, progress and prospects. Int Mat Rev. 2018; 64(6):355–380. https://doi.org/10.1080/09506608.2018.1516713
2. Melissa K, Akid R, Engelberg D, Cook T. Localised corrosion of Ni-base superalloys in seawater. 2019. [PhD thesis]. The University of Manchester, United Kingdom.
3. Crook P. Corrosion of nickel and nickel-base alloys. In: ASM Handbook, Volume 13B: Corrosion: Materials. Materials Park, OH: ASM International; 2005. p. 228–251. https://doi.org/10.31399/asm.hb.v13b.a0003821
4. Reed RC. The Superalloys: Fundamentals and applications, Cambridge University Press; 2009. https://doi.org/10.1017/CBO9780511541285
5. Jagadeesh S, Pandiarajan PS, Kumarappan J, Karthika, Karthikayan PN, Devaraj R. Enhancing energy efficiency in WSN through multiple cluster head selection and fuzzy logic. Paper presented at: 2024 International Conference on Advances in Modern Age Technologies for Health and Engineering Science (AMATHE); 2024 May 16-17; Shivamogga, India. https://doi.org/10.1109/AMATHE61652.2024.10582197
6. Dai Z, Zhou J, Wang X, Zhao T, Guo L, Yu Q. High-quality surface preparation of Inconel 718 nickel-based superalloy considering chemical mechanical polishing. Int J Prec Eng Manufact Green Technol. 2025; 13:49–64. https://doi.org/10.1007/s40684-025-00746-9
7. Das S. The national policy of biofuels of India – A perspective. Energy Policy. 2020; 143:111595. https://doi.org/10.1016/j.enpol.2020.111595
8. Shi Q, Abdel-Hamid AM, Sun Z, Cheng Y, Tu T, Cann I, *et al.* Carbohydrate-binding modules facilitate the enzymatic hydrolysis of lignocellulosic biomass: Releasing reducing sugars and dissociative lignin available for producing biofuels and chemicals. Biotechnol Adv. 2023; 65:108126. https://doi.org/10.1016/j.biotechadv.2023.108126 PMid:36921877
9. Fazal MA, Haseeb ASMA, Masjuki HH. Biodiesel feasibility study: An evaluation of material compatibility; performance; emission and engine durability. Renew Sustain Energy Rev. 2011; 15(2):1314–1324. https://doi.org/10.1016/j.rser.2010.10.004
10. Kaul S, Saxena RC, Kumar A, Negi MS, Bhatnagar AK, Goyal HB, *et al.* Corrosion behavior of biodiesel from seed oils of Indian origin on diesel engine parts. Fuel Process Technol. 2007; 88(3):303-307. https://doi.org/10.1016/j.fuproc.2006.10.011
11. Hu E, Xu Y, Hu X, Pan L, Jiang S. Corrosion behaviors of metals in biodiesel from rapeseed oil and methanol. Renew Energy. 2012; 37(1):371-378. https://doi.org/10.1016/j.renene.2011.07.010
12. Komariah LN, Arita S, Prianda BE, Dewi TK. Technical assessment of biodiesel storage tank: A corrosion case study. J King Saud Univ Eng Sci. 2023; 35(3):232-237. https://doi.org/10.1016/j.jksues.2021.03.016
13. Meenakshi HN, Shyamala R. Effect of flow and dissolved oxygen on the compatibility of *Pongamia pinnata* biodiesel with common construction materials used in storage and transportation. Int J Chem Eng. 2015; 2015:463064. https://doi.org/10.1155/2015/463064
14. Farh HMH, Seghier MEAB, Taiwo R, Zayed T. Analysis and ranking of corrosion causes for water pipelines: A critical review. NPJ Clean Water. 2023; 6(1):1-17. https://doi.org/10.1038/s41545-023-00275-5
15. Baena LM, Calderón JA. Effects of palm biodiesel and blends of biodiesel with organic acids on metals. Heliyon. 2020; 6(5):e03735. https://doi.org/10.1016/j.heliyon.2020.e03735
16. Kovács A, Tóth J, Isaák G, Kereszténvi I. Aspects of storage and corrosion characteristics of biodiesel. Fuel Process Technol. 2015; 134:59-64. https://doi.org/10.1016/j.fuproc.2015.01.014

17. Zhou J, Xiong Y, Gong Y, Liu X. Analysis of the oxidative degradation of biodiesel blends using FTIR, UV-Vis, TGA and TD-DES methods. Fuel. 2017; 202:23-28. https://doi.org/10.1016/j.fuel.2017.04.032

18. Atal S, Shukla S, Kumar S, Upadhyay SM, Hirani H, Obot IB, *et al*. Mitigation of corrosion-induced equipment loss in carbon steel in process industries using an indigenously developed acidic vapour-resistant primer. J Loss Prev Process Ind. 2026; 102:106005. https://doi.org/10.1016/j.jlp.2026.106005

19. Benitez DAN, Galvez AKL, Sesenes RL, Arteaga AMR, Rodriguez JGG. Corrosion inhibition of aluminum in a diesel-biodiesel fuel blend using *Thymus vulgaris*. Green Chem Lett Rev. 2025; 18(1). https://doi.org/10.1080/17518253.2025.2525085

20. Frankel GS. Pitting corrosion of metals: A review of the critical factors. J Electrochem Soc. 1998; 145(6):2186-2198. https://doi.org/10.1149/1.1838615

21. Wang C, Chen S, Yang X, Li L. Investigation of chloride-induced pitting processes of iron in the H_2SO_4 solution by the digital holography. Electrochem Commun. 2004; 6(10):1009-1015. https://doi.org/10.1016/j.elecom.2004.07.020

22. Cruz V, Chao Q, Birbilis N, Fabijanic D, Hodgson PD, Thomas S. Electrochemical studies on the effect of residual stress on the corrosion of 316L manufactured by selective laser melting. Corros Sci. 2020; 164:108314. https://doi.org/10.1016/j.corsci.2019.108314

23. Prajapati AK, Yadawa Y, Dwivedi D, Kumar R. Fuel property enhancement of Jatropha biodiesel by blending with nanoparticles. Chem Eng Technol. 2024; 47(1):200-207. https://doi.org/10.1002/ceat.202300150

24. Prajapati AK, Saini A, Atal S, Kumar S, Mani G, Vellaichamy RP, *et al*. Assessing the effect of different biodiesels on corrosion of nickel alloy. Mater Today Sustain. 2024; 28:100968. https://doi.org/10.1016/j.mtsust.2024.100968

25. Freire EC, García AT, Redroban C, Vega JC, Rodríguez FG. Efficiency of conventional method of protection against corrosion in ASTM A36 steels in saline medium. ESPOCH Congr Ecuador J STEAM. 2024; 3(3):179-192. https://doi.org/10.18502/espoch.v3i3.16621

26. Sterpu AE, Simedrea BG, Chis TV, Săpunaru OV. Corrosion effect of biodiesel-diesel blend on different metals/alloy as automotive components materials. Fuels. 2024; 5(1):17-32. https://doi.org/10.3390/fuels5010002

27. Hu E, Xu Y, Hu X, Pan L, Jiang S. Corrosion behaviors of metals in biodiesel from rapeseed oil and methanol. Renew Energy. 2012; 37(1):371-378. https://doi.org/10.1016/j.renene.2011.07.010

28. Onyeachu BI, Oguzie EE, Ukaga IC, Njoku DI, Peng X. Ni corrosion product layer during immersion in a 3.5% NaCl solution: Electrochemical and XPS characterization. Port Electrochim Acta. 2017; 35(3):127-136. https://doi.org/10.4152/pea.201703127

29. Yang WJ, Guo J, Li J, Zhang G, He LQ, Zhou KC. A self-repairing cermet anode: Preparation and corrosion behavior of (Cu-Ni-Fe)/$NiFe_2O_4$ cermet with synergistic action. J Am Ceram Soc. 2017; 100(3):887-893. https://doi.org/10.1111/jace.14622

30. Chaudhry AU, Mittal V, Mishra B. Nano nickel ferrite ($NiFe_2O_4$) as anti-corrosion pigment for API 5L X-80 steel: an electrochemical study in acidic and saline media. Dyes Pigm. 2015; 118:18-26. https://doi.org/10.1016/j.dyepig.2015.02.023

31. Chigane M, Ishikawa M. XRD and XPS characterization of electrochromic nickel oxide thin films prepared by electrolysis-chemical deposition. J Chem Soc Faraday Trans. 1998; 94(24):3665-3670. https://doi.org/10.1039/a806459h

32. Chandran D, Ng HK, Lau HLN, Gan S, Choo YM. Investigation of the effects of palm biodiesel dissolved oxygen and conductivity on metal corrosion and elastomer degradation under novel immersion method. Appl Therm Eng. 2016; 104:294-308. https://doi.org/10.1016/j.applthermaleng.2016.05.044

33. Ahmmad MS, Bin Haji Hassan M, Kalam MA. Comparative corrosion characteristics of automotive materials in Jatropha biodiesel. Int J Green Energy. 2018; 15(6):393-399. https://doi.org/10.1080/15435075.2018.1464925

34. Brandão JA, Seabra JHO, Castro J. Surface initiated tooth flank damage. Part II: Prediction of micropitting initiation and mass loss. Wear. 2010; 268(1-2):13-22. https://doi.org/10.1016/j.wear.2009.07.020

35. Vogiatzis CA, Kountouras DT, Skolianos SM. Corrosion behaviour of 304 stainless steel in simulated oilfield produced water. Corros Eng Sci Technol. 2016; 51(1):51-59. https://doi.org/10.1179/1743278215Y.0000000033

36. Sure J, Gill S, Wang Y, Bawane Kaustubh K, He L, Halstenberg P, *et al*. Electrochemical noise studies on localized corrosion of Ni and Ni-20Cr in molten

$ZnCl_2$. Electrochim Acta. 2022; 431:141126.. https://doi.org/10.1016/j.electacta.2022.141126

37. Alves SM, Dutra-Pereira FK, Bicudo TC. Influence of stainless steel corrosion on biodiesel oxidative stability during storage. Fuel. 2019; 249:73-79. https://doi.org/10.1016/j.fuel.2019.03.097
38. Vogiatzis CA, Kountouras DT, Skolianos SM. Corrosion behaviour of 304 stainless steel in simulated oilfield produced water. Corrosion Engineering, Science and Technology. 2016; 51(1):51-59. https://doi.org/10.1179/1743278215Y.0000000033
39. Atal S, Pandey SK, Upadhyay SM, Kumar S, Sanjay T, Hirani H, *et al.* Enhanced Tribological and Corrosion Performance of Lubricants Using Eco-Engineered Layered Double Hydroxide-Based Hybrid Additives. Journal of Tribology. 2026; 148(12):122201. https://doi.org/10.1115/1.4072514

Authors Contribution

Siddharth Atal: Conceptualisation, data curation, formal analysis, investigation, editing. Ajeet Kumar Prajapati: Conceptualisation, data curation, formal analysis, investigation, writing — original draft. Pranav Kumar: Conceptualisation, Data Curation, Software, Writing – original draft. Saurabh Kumar: Data analysis and investigation. Kuncha Swaraj: Data curation, formal analysis. Harish Hirani: Review and suggestions. Rakesh Kumar: Resources, Project administration, review and Editing. Deepak Dwivedi: supervision, conceptualisation, methodology, validation, formal analysis, investigation, writing and reviewed, editing, funding acquisition.